# IMPACT OF CHEMICAL REACTION ON MHD BOUNDARY LAYER FLOW OF NANOFLUIDS OVER A NONLINEAR STRETCHING SHEET WITH THERMAL RADIATION HAAR WAVELET COLLOCATION METHOD

#### Mahesh Kumar N

Department of Mathematics Rani Channamma University, Belagavi, India Email: maheshkumarnmk98@gmail.com

#### Vishwanath B Awati

Department of Mathematics Rani Channamma University, Belagavi, India Email: awati.vb@rcub.ac.in

#### Akash Goravar

Department of Mathematics Rani Channamma University, Belagavi, India Email: akash050992@gmail.com

## **ABSTRAK**

Reaksi yang terjadi selama perjalanan fluida melalui lapisan batas belum sepenuhnya terungkap. Situasi ini mengarah pada investigasi efek reaksi kimia dan radiasi termal pada aliran fluida lapisan batas MHD dari fluida nano yang bergerak di atas lembaran yang diregangkan secara nonlinier melalui pendekatan semi numerik. Investigasi efek reaksi kimia dan radiasi termal pada aliran fluida lapisan batas MHD dari fluida nano yang bergerak di atas lembaran yang diregangkan secara nonlinier melalui pendekatan semi numerik mencoba menemukan model fisik fluida nano dari masalah tersebut yang terdiri dari efek termoforesis, radiasi, dan parameter reaksi kimia. Model matematika yang meneliti massa, momentum, perpindahan panas, dan persamaan konsentrasi direduksi menjadi pasangan persamaan diferensial biasa nonlinier pada domain tak hingga dengan menggunakan variabel kemiripan yang tepat. Metode kolokasi *Haar wavelet* digunakan untuk menyelesaikan persamaan yang dihasilkan. Hasil yang diperoleh dibandingkan dengan temuan numerik yang tersedia dan sebanding yang mengonfirmasi dan memverifikasi metode wavelet. Efek dari berbagai parameter nondimensional pada laju perpindahan panas dan massa digambarkan melalui tabel dan grafik. Hal ini memprediksi bahwa, bilangan Sherwood lokal meningkat dengan meningkatnya parameter gerak Brown dan termoforesis. Untuk profil fraksi temperatur dan volume menurun karena peningkatan bilangan Schmidt.

Kata kunci: MHD, reaksi kimia, lembaran peregangan, radiasi termal, *Haar wavelet* 

#### **ABSTRACT**

Reactions occur during fluid passage through the boundary layer that has not been fully revealed. The situation led to investigating the effects of chemical reactions and thermal radiation on the MHD boundary layer fluid flow of a nanofluid traveling over a nonlinearly stretching sheet through a semi-numerical approach. Investigation of the effects of chemical reaction and thermal radiation on MHD boundary layer fluid flow of nanofluid moving over a nonlinearly stretching sheet through a semi-numerical approach tries to find the nanofluid physical model of the problem comprised with effects of thermophoresis, radiation, and chemical reaction parameters. The mathematical model scrutinizes mass, momentum, heat transfer, and concentration equations, which are reduced to a couple of nonlinear ordinary differential equations over an infinite domain using proper similarity variables. The Haar wavelet collocation method is used to solve the resulting equations. The obtained results are compared with available numerical findings and are comparable, which confirms and verifies the wavelet method. The effects of various non-dimensional parameters on the heat and mass transfer rate are depicted through tables and graphs. It predicts that the local Sherwood number increases with an increase in Brownian motion parameters and thermophoresis parameters. For both temperature and volume fraction profiles, it decreases due to the rise in the Schmidt number.

Keywords: MHD, chemical reaction, stretching sheet, thermal radiation, Haar wavelet

# 1. INTRODUCTION

The study of boundary layer flow over a stretching surface has significant impact on numerous engineering processes with enormous industrial applications viz. hot-rolling, glass fiber, paper production, melt spinning,

manufacture of rubber, plastic sheets, cooling of metallic sheets or electronic chips and artificial fibers etc. The quality of the final product depends on heat transfer rate and therefore the cooling procedure must be controlled effectively. Blasius type of flow in the boundary layer was investigated by Sakiadas [1]. Crane [2] deliberated the closed form solution of boundary layer flow over a stretching surface. On a stretching sheet, Wang [3] examined the convective flow and derived an analytical solution for velocity which is directly proportional to distance from the slit in a stretching sheet problem. Vajaravelu [4] employed fourth order Runge-Kutta integration scheme to obtain the solution for viscous flow over a nonlinearly stretching sheet. Hayat et al. [5] presented the solution of convection flow using Homotopy perturbation method, over a nonlinearly stretching sheet comprising micro polar fluid. Cortell [6] used similarity solutions for the flow and heat transfer of a quiescent fluid over a nonlinearly stretching sheet. Sachdev et al. [7] determined the solution of various problems arising in boundary layer flows from stretching sheets through semi-numerical approaches. Awati [8] presented the series solution of a nanofluid boundary layer over a moving semi infinite plate.

Nanofluid contains a base fluid and nano particles between 1 and 100 nm in diameter. The term 'nanofluid' was coined by Choi [9]. Nanofluids are used to enhance thermal conductivity of base fluids like water, glycol and ethylene etc. The nanofluids gained the reputation due to numerous applications and exhibited the way to a class of heat transfer fluid. Malvandi et al.[10] explored the boundary layer flow of heat transfer of nanofluid induced by a non-linearly stretching sheet. Eldable et al.[11] inspected the effect of heat generation and magnetic field on viscous nanofluid flow of heat transfer over a nonlinearly stretching surface. The influence of convective boundary layer flow of a nanofluid over a nonlinearly stretching sheet with boundary conditions was scrutinised by Makinde and Aziz [12]. Rana and Bhargava [13] examined heat transfer of nanofluid flow over a nonlinear stretching sheet using finite element and finite difference schemes. Mabood et al.[14] studied heat transfer effect on magnetohydrodynamic (MHD) boundary layer flow in existence of nanofluid over a nonlinear stretching sheet using Runge Kutta method. Rashidi et al. [15] scrutinize the convective heat transfer of nanofluid flow over a stretching sheet by using Keller box method. Khan and Pop [16] numerically discussed the boundary layer flow of a nanofluid. Gorla and Sidawai [17] illustrated the free convection on a vertical stretching sheet by Keller box method. Ramya et al.[18] presented the influence of chemical reaction on MHD boundary layer flow of nanofluid over a stretching sheet with thermal radiation. Awati and Mahesh [19] examined the static and moving flat plate due to forced convection boundary layer flow and heat transfer with nanofluid by using Haar wavelet. Awati et al. [20] semi-numerically inspected the features of heat and mass transfer of convective boundary layer flow of a nanofluid moving over nonlinear stretching surface.

Chemical reactions are defined as either heterogeneous or homogeneous processes. It depends on whether they occur as an interface or as single-phase volume reaction effects. The study of heat transfer with chemical reaction on nanofluids in the existence of thermal radiation parameters has immense genuine importance to engineers and scientists, because of its universal prevalence in many branches of engineering and science. This frequently occurs in petro-chemical industry, cooling systems, power and chemical vapour deposition on surfaces, heat exchanger design, cooling of nuclear reactors, geophysics and forest fire dynamics as well as MHD power generation systems. Reddy and Sreedevi [21] illustrated the impact of chemical reaction and double stratification on heat and mass transfer characteristics of nanofluid flow over porous stretching sheets with thermal radiation. Rapits and Perdikis [22] conducted similar research on viscous flow over a nonlinear stretching sheet in presence of a chemical reaction and magnetic field. Chemical reaction and uniform heat generation effects on the stagnation point flow of a nanofluid on MHD over a porous sheet were investigated by Anwar et al.[23] using Keller box method. Electrically-conducting nanofluid flows, which respond to the imposition of magnetic fields have received relatively major consideration. The solution of the boundary layer equation for a power law fluid in magneto-hydrodynamics is discussed by Helmy [24], Whereas, Chiam [25] scrutinized the hydro-magnetic flow over a surface stretching with a power-law velocity using shooting technique. Ishak et al. [26] inspected the hydromagnetic flow and heat transfer adjacent to a stretching vertical sheet. Nourazar et al. [27] presented the MHD forced-convective flow of nanofluid over a horizontal stretching flat plate with variable magnetic field including viscous dissipation. Zeeshan et al. [28] examined the MHD flow of third-grade nanofluid between coaxial porous cylinders whilst Chamkha and Aly [29] considered the MHD free convective boundary-layer flow of a nanofluid with a permeable isothermal vertical plate in the occurrence of heat source or sink. MHD mixed convective boundary layer flow of nanofluid over a stretching sheet was examined by Matin et al. [30]. Recently Awati et al. [31] discussed mass transfer on a continuous flat plate moving in parallel to a free stream in the presence of a chemical reaction through the Chebyshev collocation method. Wakif et al. [32] demonstrated the onset of convection in a horizontal nanofluid layer of finite depth via Wakif-Galerkin weighted residuals technique.

Haar wavelet Collocation method (HWCM) is one of the most sophisticated semi-numerical methods which is widely used for the solution of differential and integro-differential equations. These Haar wavelets are generated from pairs of piecewise constant functions. According to Lepik [33] there are two main benefits that overwhelmed the difficulties of solving nonlinear differential equations using other pure numerical methods. The first benefit is that the quadratic waves can be legalised with interpolating splines etc. and the second one; the

highest order derivative incorporated in the differential equation is expanded into a series of Haar functions. Lepik [34] determined the Haar wavelet discretization method (HWDM) for solving large classes of differential, fractional differential and integro-differential equations including problems from elasto-static, mathematical physics, non-linear oscillations and evolution equations. Majak et al. [35] obtained the convergence theorem for HWDM, the order of convergence as well as error bounds of Haar wavelet method is proved for general nth order ordinary differential equations. Also, anticipated that the order of convergence is, in equations 1:

$$O\left[\left(\frac{1}{2^{J+1}}\right)^2\right] \tag{1}$$

where J is the resolution level

In the present study, the impact of chemical reaction on MHD boundary layer flow of nanofluid over a nonlinear stretching sheet with thermal radiation is analysed. The governing self-similar equations are solved through an elegant semi-numerical approach by using HWCM. The effects of various parameters involved in the self-similar equations are discussed in detail and presented the results through tables and figures.

## 2. METHOD

## 2.1. Mathematical Formulation

Consider a two-dimensional incompressible and steady viscous fluid flow of a water-based nanofluid flow past a nonlinear stretching surface. The sheet is extended with velocity with fixed origin, where n is a nonlinear stretching parameter, a is a constant, and x is the coordinate measured along the stretching surface. The nanofluid flows at where the y-axis is normal to the surface. The fluid is electrical conducting due to an applied magnetic field B(x) normal to the stretching sheet. The magnetic Reynolds number is assumed to be small and so, the induced magnetic field is considered to be negligible. The wall temperature and nanoparticle fraction are assumed to be constant at the stretching surface. When y tends to infinity, the ambient temperature and nanoparticle fraction are denoted by and, respectively. The geometry of the problem is shown in Figure 1.

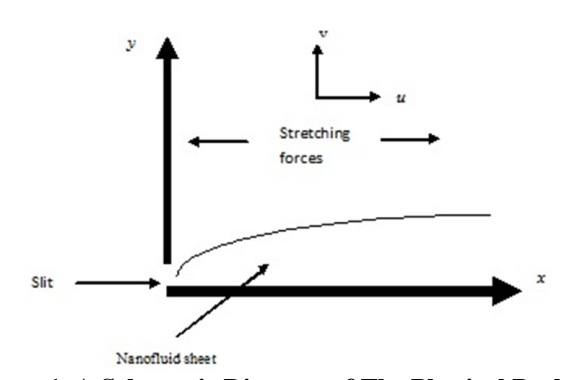


Figure 1. A Schematic Diagram of The Physical Problem

The governing physical equations of the mathematical modeling can be written as [18]

$$\frac{\partial u}{\partial x} + \frac{\partial v}{\partial y} = 0,\tag{2}$$

$$u\frac{\partial u}{\partial x} + v\frac{\partial u}{\partial y} = v\frac{\partial^2 u}{\partial y^2} - \frac{\sigma B^2(x)}{\rho_f}u,\tag{3}$$

$$u\frac{\partial T}{\partial x} + v\frac{\partial T}{\partial y} = \alpha \frac{\partial^2 T}{\partial y^2} + \tau \left\{ D_B \frac{\partial C}{\partial y} \frac{\partial T}{\partial y} + \frac{D_T}{T_\infty} \left( \frac{\partial T}{\partial y} \right)^2 \right\} + \frac{v}{c_p} \left( \frac{\partial u}{\partial y} \right)^2 - \frac{1}{\left( \rho_{cp} \right)_f} \frac{\partial q_r}{\partial y}, \tag{4}$$

$$u\frac{\partial C}{\partial x} + v\frac{\partial C}{\partial y} = D_B \frac{\partial^2 C}{\partial y^2} + \left(\frac{D_T}{T_\infty}\right) \frac{\partial^2 T}{\partial y^2} - K_r \left(C - C_\infty\right),\tag{5}$$

The boundary conditions for velocity, temperature and nanoparticle functions becomes [18]

$$y = 0: u_W = ax^n, \ v = 0, \ T = T_W, \ C = C_W$$
 (6)

$$y \to \infty$$
,  $u = 0$ ,  $v = 0$ ,  $T = T_{\infty}$ ,  $C = C_{\infty}$  (7)

where

(u, v) denotes the velocity components along the x and y directions,

 $\alpha = K/(\rho c)_f$  is the thermal diffusivity

 $\tau = (\rho c)_p/(\rho c)_f$  is the ratio between the effective heat capacity of nanoparticle material and the heat capacity of the ordinary fluid

 $D_T$  is the Brownian diffusion coefficient

 $D_B$  is the thermophoresis diffusion coefficient

 $B(x) = B_0 x^{(n-1)/2}$  is the variable magnetic field, where  $B_0$  is constant

Using Rosseland's approximation for radiation becomes

$$q_r = -\frac{4\sigma^*}{3k^*} \frac{\partial T^4}{\partial y} \tag{8}$$

where  $k^*$  is the absorption coefficient,  $\sigma^*$  is the Stefan-Boltzman constant. Let us assume that, the temperature difference within the flow is such that  $T^4$  may be expanded in a Taylor series  $T_\infty$  and neglects the higher orders, we get  $T^4 \approx 4T_\infty^3 T - 3T_\infty^4$ . Hence Equation (8) becomes

$$\frac{\partial q_r}{\partial y} = -\frac{16\sigma^* T_\infty^2}{3(\rho_{cD})_f k^*} \frac{\partial^2 T}{\partial y^2} \tag{9}$$

The similarity variable exists for Equations (2) to (7) and introduces the following similarity variables [18] as

$$\eta = y \sqrt{\frac{a(n+1)}{2\nu}} x^{(n-1)/2} \,, \\ u = a x^n f'(\eta) \,, \ v = -\sqrt{\frac{a \nu (n+1)}{2}} x^{(n-1)/2} \left( f(\eta) + \frac{n-1}{n+1} \eta f'(\eta) \right), \ \theta(\eta) = \frac{T - T_{\infty}}{T_W - T_{\infty}} \,, \\ \theta(\eta) = \frac{T - T_{\infty}}{T_W - T_{\infty}} \,.$$

$$\varphi(\eta) = \frac{C - C_{\infty}}{C_W - C_{\infty}} \tag{10}$$

The stream function  $\psi$  is defined as  $u = \partial \psi / \partial y$ ,  $v = \partial \psi / \partial x$ , so Equation (2) satisfies automatically, and Equations (3)-(5) are simplified by using Equation (10); we get

$$f''' + ff'' - \frac{2n}{n+1}f'^2 - Mf' = 0 \tag{11}$$

$$\frac{1}{\Pr}\left(1 + \frac{4}{3}R\right)\theta'' + f\theta' + Nb\varphi'\theta' + Nt\theta'^2 + Ecf''^2 = 0\tag{12}$$

$$\varphi'' + Lef \varphi' + \frac{Nt}{Nb} \theta'' - \gamma Le \varphi = 0$$
(13)

The relevant boundary conditions become

$$f(0) = 0$$
,  $f'(0) = 0$ ,  $\theta(0) = 1$ ,  $\varphi(0) = 1$ ,

$$f'(\infty) = 0 , \quad \theta(\infty) = 0 , \quad \varphi(\infty) = 0$$
 (14)

where

The prime denotes the differentiation with respect to  $\eta$ .

The physical parameters are defined as Magnetic parameter  $M = \frac{2\sigma B_0^2}{a\rho_f(n+1)}$ ,

Brownian motion parameter  $Nb = \frac{(\rho c)_p D_B (C_W - C_\infty)}{(\rho c)_f V}$ ,

Thermophoresis parameter  $Nt = \frac{(\rho c)_p D_T (T_W - CT_\infty)}{(\rho c)_f v T_\infty}$ ,

Radiation parameter  $R = \frac{4\sigma^* T_{\infty}^3}{kk^*}$ ,

Prandtl number  $Pr = \frac{v}{\alpha}$ ,

Eckert number  $Ec = \frac{u_W^2}{c_p(T_w - T_\infty)}$ ,

Lewis number  $Le = \frac{v}{D_B}$  and Chemical reaction parameter

$$\gamma = \frac{2k_1}{a(n+1)(C_W - C_\infty)} x^{\frac{(n-1)}{2}}$$
 (15)

The local skin-friction, Nusselt number, and Sherwood numbers are defined as

$$C_{fx} = \frac{\mu_f}{\rho u_W^2} \left[ \frac{\partial u}{\partial y} \right]_{y=0}, \quad Nu_x = \frac{xq_W}{k(T_W - T_\infty)}, \quad Sh_x = \frac{xq_m}{D_B(C_W - C_\infty)}$$
(16)

where k is the thermal conductivity of nanofluid and  $q_W$ ,  $q_m$  the heat and mass fluxes at the surfaces are given by

$$q_W = -\left[\frac{\partial T}{\partial y}\right]_{y=0}, \quad q_m = -D_B\left[\frac{\partial C}{\partial y}\right]_{y=0}$$
 (17)

Substituting Equation (7) into Equations. (16)-(17), we obtain

$$\operatorname{Re}_{x}^{1/2} C f_{x} = \sqrt{\frac{n+1}{2}} f''(0), \quad \operatorname{Re}_{x}^{1/2} N u_{x} = \sqrt{\frac{n+1}{2}} \theta'(0), \quad \operatorname{Re}_{x}^{1/2} S h_{x} = \sqrt{\frac{n+1}{2}} \phi'(0)$$
(18)

Where  $\text{Re}_x = u_W x / v$  is the local Reynolds number. Equations (11) - (13) are nonlinear, hence it is amenable to get the closed form solution. Consequently, these nonlinear equations Equations (11) to (13) with the boundary conditions (14) are solved semi-numerically by means of Haar wavelet collocation method.

# 2.2. Haar wavelet procedure

Lepik [31], defines the notation of family of Haar wavelets, let us consider the domain of integration  $\eta \in [A, B]$ , where A and B are constants. Define  $M = 2^J$ , where J denotes the resolution of maximal

level. The domain [A, B] is divided into 2M subintervals of equal length i.e. the length of each subinterval is  $\Delta \eta = (B - A)/2M$ , the  $i^{th}$  Haar wavelet is the group of square waves with  $\pm 1$  as the magnitude in the relevant interval and elsewhere it becomes zero.

$$h_{i}(\eta) = \begin{cases} 1, & \text{for } \eta \in \left[\zeta_{1}(i), \zeta_{2}(i)\right), \\ -1, & \text{for } \eta \in \left[\zeta_{2}(i), \zeta_{3}(i)\right), \\ 0, & \text{elsewhere.} \end{cases}$$

$$(19)$$

where

$$\zeta_1(i) = A + 2k \mu \Delta \eta$$
,  $\zeta_2(i) = A + (2k+1)\mu \Delta \eta$ ,  $\zeta_3(i) = A + 2(k+1)\mu \Delta \eta$ ,  $\mu = M/m$ , for  $j = 0, 1, 2,....M$  and  $k = 0, 1, 2,...M - 1$  respectively denotes the parameters of dilation and translation.

The subscript i can be calculated as i = m + k + 1. The parameter  $m = 2^j$  ( $M = 2^J$ ) represents the number of maximum square waves that can be sequentially placed in [A, B] and the parameter k specifies the location of the particular square wave. For i=1, the scaling function of Haar wavelet becomes

$$h_{\mathbf{I}}(\eta) = \begin{cases} 1, & \eta \in [A, B), \\ 0, & elsewhere. \end{cases}$$
 (20)

To construct a relevant transform basis by using the orthogonality of Haar wavelet functions as

$$\int_{0}^{1} h_{i}(x)h_{l}(x)dt = \begin{cases} 2^{-j}, & i = l = 2^{j} + k \\ 0, & i \neq l \end{cases}$$
 (21)

For any finite, square-integrable function f(x) in [A, B] can be expressed in terms of Haar wavelets as

$$f(x) = \sum_{i=1}^{\infty} a_i h_i(x), \tag{22}$$

where  $a_i$  are the Haar coefficients

$$a_i = 2^j \int_A^B f(x) h_i(x) dx, \quad i = 1, 2, \dots, 2^j + k + 1.$$
 (23)

The coefficients of Haar wavelet are obtained from the minimum condition of integral square error as

$$\int_{A}^{B} E_{M}^{2} dx \to \min, \qquad \left| E_{M} \right| = \left| f\left(x\right) - f_{M}\left(x\right) \right|, \quad f_{M}\left(x\right) = \sum_{i=0}^{2M} a_{i} h_{i}\left(x\right), \tag{24}$$

where f(x) and are the exact and approximate solutions respectively. Analytically, the integrals of Equation (17) of order n can be determined as

$$p_{n,i} = \int_{n-times}^{\eta} \int_{n-times}^{\eta} h_i(x)dx^n = \frac{1}{(n-1)!} \int_{A}^{\eta} (t-x)^{n-1} h_i(x)dx$$
(25)

where n = 1, 2, ..., N and i = 1, 2, ..., 2M. The case n = 0 corresponds to function  $h_i(\eta)$ . By the definition, the integrals may be calculated as

$$p_{n,i}(\eta) \begin{cases} 0, & for \ \eta \in [A, \zeta_{1}(i)), \\ \frac{1}{n!} [\eta - \zeta_{1}(i)]^{n}, & for \ \eta \in [\zeta_{1}(i), \zeta_{2}(i)) \end{cases} \\ \frac{1}{n!} \{ [\eta - \zeta_{1}(i)]^{n} - 2[\eta - \zeta_{2}(i)]^{n} \}, & for \ \eta \in [\zeta_{2}(i), \zeta_{3}(i)), \\ \frac{1}{n!} \{ [\eta - \zeta_{1}(i)]^{n} - 2[\eta - \zeta_{2}(i)]^{n} + [\eta - \zeta_{3}(i)]^{n} \}, & for \ \eta \in [\zeta_{3}(i), B). \end{cases}$$

$$(26)$$

This formula holds for i > 1, in the case i = 1, we have  $\zeta_1 = A$ ,  $\zeta_2 = \zeta_3 = B$  and

$$p_{n,1}(\eta) = \frac{1}{n!} (\eta - A)^n \tag{27}$$

The collocation points are  $\eta_l = 0.5(\overline{\eta}_l + \overline{\eta}_{l-1})$ , l = 1, 2, ..., 2M. The symbol  $\overline{\eta}_l$  denotes the l <sup>th</sup>grid point  $\overline{\eta}_l = A + l\Delta \eta$ ,  $l = 1, 2, \ldots, 2M$ .

## 2.3. Solution by HWCM

We seek higher-order derivatives of Equation (11) in the form of Haar wavelet approximation as

$$f'''(\eta) = \sum_{i=1}^{2M} a_i h_i(\eta), \tag{28}$$

where  $a_i$  are the Haar wavelet coefficients. The corresponding lower-order derivatives are derived using Equation (11) with (14), we have

$$f''(\eta) = f''(0) + \sum_{i=1}^{2M} a_i p_{1,i}(\eta)$$
(29)

$$f'(\eta) = 1 + \eta f''(0) + \sum_{i=1}^{2M} a_i p_{2,i}(\eta).$$
(30)

$$f(\eta) = \eta + \frac{\eta^2}{2} f''(0) + \sum_{i=1}^{2M} a_i p_{3,i}(\eta).$$
(31)

Letting  $\eta_{\infty} = B$  and, using relevant conditions (12), we obtain

$$f''(0) = \frac{-1}{B} \left[ 1 + \sum_{i=1}^{2M} a_i \, \mathcal{C}_i^1 \, . \right] \tag{32}$$

where  $C_i^1 = \int_A^B p_{1,i}(x) dx$ . Substitution of Equations (28) to (32) into Equations (11) becomes the following nonlinear system of equations.

$$\sum_{i=1}^{2M} a_{i} H(i,l) + \left\{ \left( \eta_{i} + \frac{\eta_{i}^{2}}{2} \left( -\frac{1}{B} \left[ 1 + \sum_{i=1}^{2M} a_{i} C \right] \right) + \sum_{i=1}^{2M} a_{i} R(i,l) \right) \right\} \left\{ -\frac{1}{B} \left[ 1 + \sum_{i=1}^{2M} a_{i} C \right] + \sum_{i=1}^{2M} a_{i} P(i,l) \right\} - \left( \frac{2n}{n+1} \right) \left( 1 + \left( \frac{\eta_{i}}{B} \left[ 1 + \sum_{i=1}^{2M} a_{i} C \right] \right) + \sum_{i=1}^{2M} a_{i} Q(i,l) \right)^{2} - M \left( 1 + \left( \frac{\eta_{i}}{B} \left[ 1 + \sum_{i=1}^{2M} a_{i} C \right] \right) + \sum_{i=1}^{2M} a_{i} Q(i,l) \right) = 0,$$

$$I = 1, 2, 3, 2^{J+1}$$
(33)

In the similar manner, we approximate higher-order derivatives in Equation (12) and (13) in terms of the Haar wavelets as

$$\theta''(\eta) = \sum_{i=1}^{2M} b_i h_i(\eta), \text{ and } \phi''(\eta) = \sum_{i=1}^{2M} c_i h_i(\eta),$$
(34)

where  $b_i$  and  $c_i$  are the coefficients of the Haar wavelet. The corresponding lower-order derivatives are derived using Equations (34) along with (14), we have

$$\theta'(\eta) = \theta'(0) + \sum_{i=1}^{2M} b_i p_{1,i}(\eta), \text{ and } \phi'(\eta) = \phi'(0) + \sum_{i=1}^{2M} c_i p_{1,i}(\eta).$$
(35)

$$\theta(\eta) = 1 + \eta \theta'(0) + \sum_{i=1}^{2M} b_i p_{2,i}(\eta), \quad \text{and} \quad \phi(\eta) = 1 + \eta \phi'(0) + \sum_{i=1}^{2M} c_i p_{2,i}(\eta).$$
(36)

Using boundary conditions (14) and letting  $\eta_{\infty} = B$ , we obtain

$$\theta'(0) = \frac{-1}{B} \left[ 1 + \sum_{i=1}^{2M} b_i C_i^i \right] \text{ and } \phi'(0) = \frac{-1}{B} \left[ 1 + \sum_{i=1}^{2M} c_i C_i^i \right]$$
(37)

Thus, by substituting Equations (34) to (36) into Equations (12) and (13), we get the nonlinear system of equations as

$$\frac{1}{\Pr}\left(1 + \frac{4}{3}R\right) \sum_{i=1}^{2M} b_i H\left(i,l\right) + \left\{ \left(\eta_i + \frac{\eta_i^2}{2} \left(\frac{-1}{B} \left[1 + \sum_{i=1}^{2M} a_i C\right]\right) + \sum_{i=1}^{2M} a_i R\left(i,l\right)\right) \left(\frac{-1}{B} \left[1 + \sum_{i=1}^{2M} b_i C\right] + \sum_{i=1}^{2M} b_i P\left(i,l\right)\right) \right\} 
+ Nb \left[ \left(\frac{-1}{B} \left[1 + \sum_{i=1}^{2M} b_i C\right] + \sum_{i=1}^{2M} b_i P\left(i,l\right)\right) \left(\frac{-1}{B} \left[1 + \sum_{i=1}^{2M} c_i C\right] + \sum_{i=1}^{2M} c_i P\left(i,l\right)\right) \right] 
+ Nt \left(\frac{-1}{B} \left[1 + \sum_{i=1}^{2M} b_i C\right] + \sum_{i=1}^{2M} b_i P\left(i,l\right)\right) + Ec \left(\left(\frac{-1}{B} \left[1 + \sum_{i=1}^{2M} a_i C\right]\right) + \sum_{i=1}^{2M} a_i P\left(i,l\right)\right) = 0,$$
(38)

And

$$\sum_{i=1}^{2M} c_{i} H(i,l) + \frac{1}{2} Le \left\{ \left( \eta_{i} + \frac{\eta_{i}^{2}}{2} \left( \frac{-1}{B} \left[ 1 + \sum_{i=1}^{2M} a_{i} C \right] \right) + \sum_{i=1}^{2M} a_{i} R(i,l) \right) \left( \frac{-1}{B} \left[ 1 + \sum_{i=1}^{2M} c_{i} C \right] + \sum_{i=1}^{2M} c_{i} P(i,l) \right) \right\} + \frac{Nt}{Nb} \left( \sum_{i=1}^{2M} b_{i} H(i,l) \right) - \gamma Le \left( 1 + \frac{-\eta_{i}}{B} \left[ 1 + \sum_{i=1}^{2M} c_{i} C \right] + \sum_{i=1}^{2M} c_{i} Q(i,l) \right) = 0,$$

$$l = 1, 2, 3, \dots, 2^{J+1},$$
(39)

Where

$$H(i,l) = h_i(\eta_l)$$
,  $P(i,l) = p_{1,i}(\eta_l)$ ,  $Q(i,l) = p_{2,i}(\eta_l)$  and  $R(i,l) = p_{3,i}(\eta_l)$  are  $2^{J+1} \times 2^{J+1}$  square matrices,  $C = (C_i^1)$  is a  $2^{J+1}$  dimensional column matrix.

The sparsity of Haar and higher integral matrices increases as the resolution levels J increase and matrix sizes also increase. The merit of this algorithm is that it decreases computational time and is faster to implement for the solution of BVPs. The unknown coefficients  $a_i$  are determined by using Newton's method.

# 3. RESULTS AND DISCUSSION

The computations were executed semi-numerically to analyze the effects of chemical reaction on MHD boundary layer flow of a nanofluid over a nonlinearly stretching sheet with thermal radiation. The transformed coupled nonlinear ordinary differential Equations (11)–(13) with pertinent infinite boundary conditions Equation (14) are solved using HWCM. The dimensionless velocity, temperature and concentration profiles were obtained and also, the local skin friction, the Nusselt number and Sherwood number are obtained. The obtained results are

presented via. Graphs and tables. The obtained solutions are compared with previously published results of Mabood et al. [14] and Ramya et al. [18], the results are comparable. In the absence of chemical reaction and thermal radiation parameters for skin friction, heat transfer rate and mass transfer rates are shown in Tables 1 and 2 and are found to be in an excellent agreement with earlier findings. It shows that the increase in nonlinear parameter n leads to Nusselt and Sherwood numbers decreasing, similar results are obtained with increase in Pr and Le. Also, skin friction coefficient increases due to increase in the Magnetic parameter, whereas Nusselt and Sherwood numbers decrease.

Table 1. Comparison of Nusselt Number and Sherwood Number when Nb = Nt = 0.5, M = Ec = 0R = 0 and  $\gamma = 0$ 

		n		<i>-θ'</i> (0)			- φ' ( <b>0</b> )			
Le	Pr		Mabood	Rana and	Present	Mabood	Rana and	Present		
2	0.7	0.2	et al[14] 0.3295	Bhargava[13] 0.3299	0.3299	et al[14] 0.8134	<b>Bhargava[13]</b> 0.8132	<b>Method</b> 0.8141		
2	0.7	0.2	0.3293	0.3299	0.3266	0.8154	0.8132	0.8074		
		3	0.3262	0.3053	0.3255	0.7633	0.7630	0.7642		
		10	0.3030	0.3002	0.3004	0.7633	0.7630	0.7536		
		20	0.2999	0.3002	0.3004	0.7527		0.7509		
		20	0.2980	0.2823	0.2991	0.7300	1.4548	0.7309		
	2.0	0.2	0.3987	0.3999	0.3987	0.8060	0.8048	0.8060		
		0.3	0.3959	0.3930	0.3959	0.7971	0.7826	0.7971		
		3	0.3775	0.3786	0.3775	0.7390	0.7379	0.7391		
		10	0.3728	0.3739	0.3728	0.7248	0.7238	0.7249		
		20	0.3716	0.3726	0.3716	0.7212	0.7201	0.7213		
	7.0	0.2	0.2222	0.2240	0.2222	1.0120	1.0114	1.0120		
	7.0	0.2	0.2223	0.2248	0.2223	1.0138	1.0114	1.0138		
		0.3	0.2229	0.2261	0.2229	1.0015	0.9808	1.0015		
		3	0.2266	0.2288	0.2266	0.9207	0.9185	0.9207		
		10	0.2274	0.2297	0.2274	0.9007	0.8985	0.9007		
		20	0.2276	0.2299	0.2276	0.8956	0.8933	0.8956		
10	0.7	0.2	0.3035	0.3042	0.3037	2.3206	2.3198	2.3215		
		0.3	0.3033	0.2965	0.3007	2.3110	2.2959	2.3119		
		3	0.2806	0.2812	0.2810	2.2471	2.2464	2.2481		
		10	0.2758	0.2765	0.2763	2.2310	2.2303	2.2320		
		20	0.2747	0.2753	0.2751	2.2268	2.2261	2.2278		
	2.0	0.2	0.2816	0.2835	0.2815	2.4227	2.4207	2.4234		
		0.3	0.2793	0.2778	0.2793	2.4112	2.2778	2.4119		
		3	0.2644	0.2661	0.2644	2.3342	2.3324	2.3349		
		10	0.2607	0.2624	0.2607	2.3148	2.3130	2.3154		
		20	0.2597	0.2614	0.2597	2.3097	2.3080	2.3104		
	<b>7</b> 0	0.0	0.0524	0.0545	0.0504	2 - 24 -		2 522-		
	7.0	0.2	0.0534	0.0547	0.0531	2.6216	2.6202	2.6227		
		0.3	0.0533	0.0546	0.0529	2.6085	2.5871	2.6096		
		3	0.0522	0.0537	0.0519	2.5210	2.5194	2.5220		
		10	0.0520	0.0534	0.0516	2.4989	2.4973	2.4998		
		20	0.0519	0.0534	0.0516	2.4932	2.4916	2.4941		

Table 2. Comparison of Skin-Friction Coefficient, Nusselt and Sherwood Numbers for Various Values of Ec and M when Pr = 6.2, Le = 5, Nb = Nt = 0.1, n = 2, R = 0, and  $\gamma = 0$ 

Ec M		<b>-f''(0)</b>			<i>-θ'</i> (0)			$-\varphi'(0)$		
	M	Mabood et al [14]	Ramya et al [18]	Present method	Mabood et al [14]	Ramya et al [18]	Present method	Mabood et al [14]	Ramya et al [18]	Present method
0		1.10102	1.10142	1.10145	1.06719	1.06713	1.06717	1.07719	1.07684	1.07679
0.1					0.88199	0.88888	0.88890	1.22345	1.22329	1.22326
0.2	0				0.70998	0.70941	0.70939	1.37078	1.37081	1.37081
0.3					0.52953	0.52869	0.52864	1.51919	1.51941	1.51944
0.5					0.16484	0.16344	0.16332	1.81933	1.81995	1.82004

Table 2. Comparison of Skin-Friction Coefficient, Nusselt and Sherwood Numbers for Various Values of Ec and M when Pr=6.2, Le=5, Nb=Nt=0.1, n=2, R=0, and  $\gamma=0$ , continued

Ec	M	f''(0)			- heta'(0)			$-\varphi'(0)$		
		Mabood et al [14]	Ramya et al [18]	Present method	Mabood et al [14]	Ramya et al [18]	Present method	Mabood et al [14]	Ramya et al [18]	Present method
0		1.30989	1.30991	1.30989	1.04365	1.04365	1.04370	1.01090	1.01090	1.01084
0.1					0.81055	0.81055	0.81057	1.20605	1.20603	1.20602
0.2	0.5				0.57564	0.57562	0.57563	1.40279	1.40279	1.40279
0.3					0.33889	0.33883	0.33886	1.60115	1.60116	1.60117
0.5					0.14022	0.14033	0.14031	2.00282	2.00287	2.00290
0		1.48912	1.48912	1.48909	1.02337	1.02337	1.02342	0.95495	0.95494	0.95492
0.1					0.74058	0.74057	0.74062	1.19496	1.19495	1.19495
0.2	1				0.45543	0.45542	0.45547	1.43706	1.43706	1.43706
0.3					0.16789	0.16788	0.16793	1.68128	1.68216	1.68128
0.5					0.41451	0.41452	0.41448	2.17623	2.17620	2.17626

Table 3. Calculation of Skin-Friction Coefficient, Nusselt and Sherwood Numbers for Various Values of R and  $\gamma$  when Pr = 6.2, Le = 5, Nb = Nt = 0.1 and n = 2.Ec = 0.1

R	γ	f''(0)	<i>-θ'</i> (0)	-φ'(0)
0.1	0.1	1.309899	0.78146	1.43776
0.3	0.1		0.75551	1.43510
0.5	0.1		0.72629	1.43929
0.9	0.1		0.66904	1.45459
1.0	0.1		0.65564	1.45885
1.0	0.2	1.309899	0.65104	1.64917
1.0	0.5		0.64124	2.11667
1.0	0.7		0.63671	2.37316
1.0	0.9		0.63315	2.60119
1.0	1.0		0.63162	2.70696

The effects of radiation and chemical reaction parameters presented in Table 3, when Pr = 6.2, Le = 5, Nb = Nt = 0.1 and n = 2 on skin-friction, Nusselt and Sherwood numbers. It reveals that the Nusselt number decreases and Sherwood number increases with various values of radiation and chemical reaction parameters. Figure 2 illustrate the effect of various magnetic parameters on  $f'(\eta)$ . It shows that the dimensionless velocity  $f'(\eta)$  profiles decreases with increase in the values of magnetic parameter M = 0, 1, 2, 3. This is due to the magnetic field exhibit a resistant body force that acts transverse to the direction of applied magnetic field. The body force is known as Lorentz force, decreases the boundary layer flow and thickens the momentum boundary layer. Figures 3 and 4 demonstrate the effect of magnetic parameter M = 0, 1, 2, 3 on the dimensionless temperature  $\theta(\eta)$  and nanoparticle concentration  $\varphi(\eta)$ , respectively. It depicts that, by increasing magnetic parameters, the dimensionless temperature and concentration profiles are significantly enhanced. As resistive Lorentz force opposes the fluid motion and heat is generated as a result, the thermal boundary layer thickness and nanoparticle volume fraction boundary layer thickness becomes too thicker.

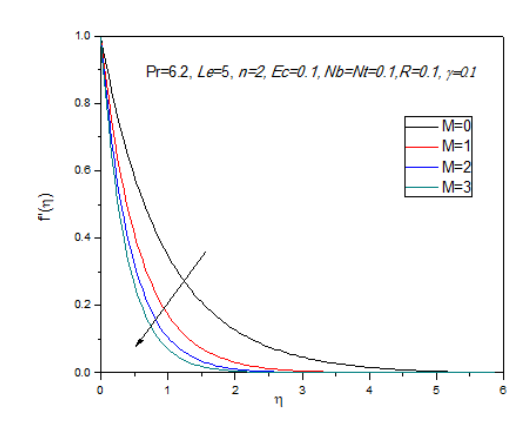


Figure 2. Variation of  $f(\eta)$  with Various Values of M

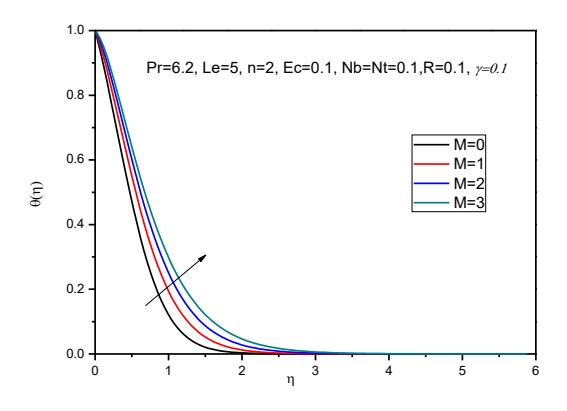


Figure 3. The Temperature Profile for Different Values of M

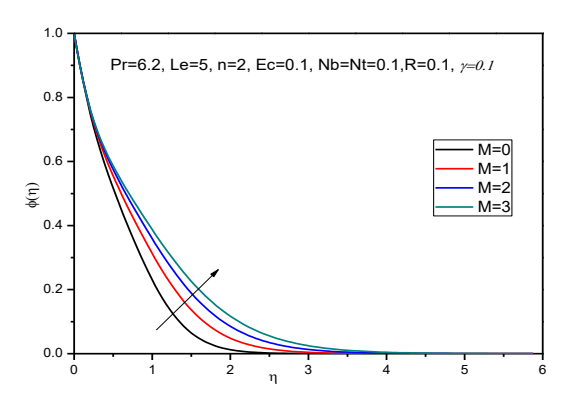


Figure 4. Effects of M on Dimensionless Concentration Profiles

Figures 5 and 6 exhibits the influence of thermophoresis parameter Nt on  $\theta(\eta)$  and  $\varphi(\eta)$  respectively. It envisages that, the dimensionless temperature  $\theta(\eta)$  and nanoparticle concentration  $\varphi(\eta)$  increases with increasing values of thermophoresis parameter Nt. This is due to thermophoretic force related to temperature gradient, which induces a fast flow away from the stretching surface. Thus, heated fluid is moved away from the stretching surface. As Nt increases, the temperature within the boundary layer increases and concentration boundary layer thickness also increases. The variation of Brownian motion parameters Nt = 0.1, 0.2, 0.3, 0.4 on  $\theta(\eta)$  and  $\varphi(\eta)$  are shown in Figures 7 and 8, respectively. It is evident that the dimensionless temperature profiles increase and concentration profiles decrease respectively with increase in the values of Nb. The thermal boundary layer becomes thicker due to increase in the values of Nb. Thus, the fluid exhibit nanoparticle concentration decreases inside the boundary layer.

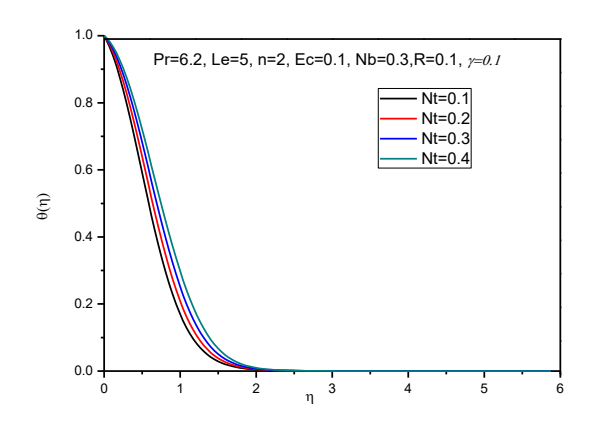


Figure 5. Effect of Nt on Dimensionless Temperature

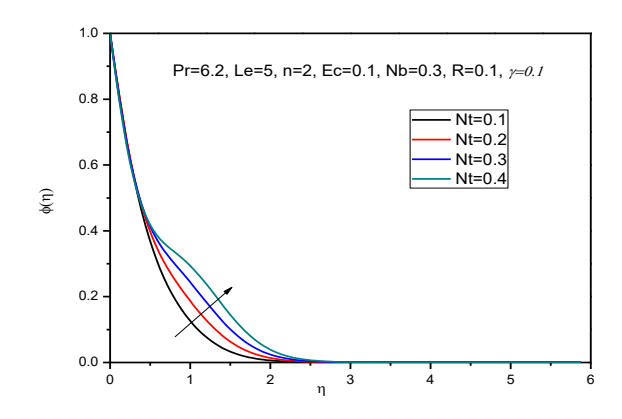


Figure 6. Effect of Nt on Dimensionless Concentration Profiles

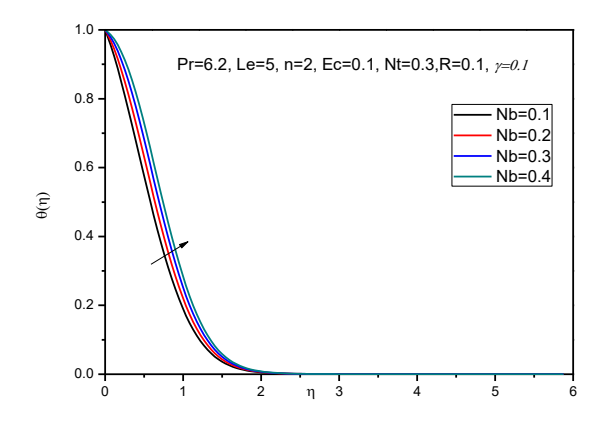


Figure 7. Effect of Nb on Dimensionless Temperature

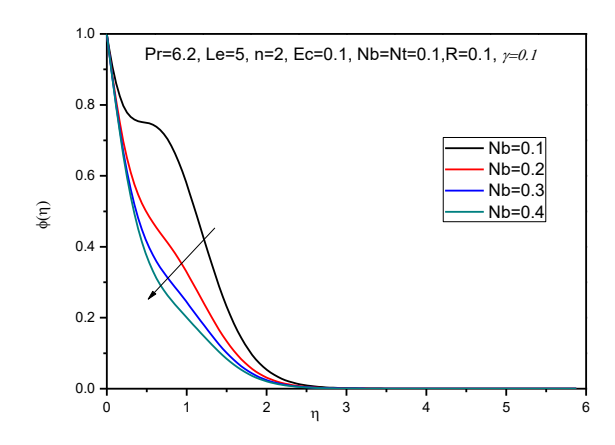


Figure 8. Effects of Nb on Dimensionless Concentration

Figure 9 illustrates the effect of Eckert number Ec on dimensionless temperature. As the viscous dissipation parameter increases, the dimensionless temperature increases. The effect of Lewis number (Le) on concentration profiles are shown in Figure 10. It shows that, by increasing the value of Le, the concentration boundary layer thickness decreases. This is due to decrease in mass diffusivity or Brownian motion of the nanoparticles. Figure 11 presents the effect of thermal radiation R and nonlinear stretching parameter n on dimensionless temperature. It predicts that the dimensionless temperature profiles of nanofluid are significantly increased with increasing values of R and n. By releasing heat energy from the flow region the thermal radiation

leads to thickening the thermal boundary layer, so it cools the system. In reality it is the fact that, because of temperature increases as a result the Rosseland expansion approximation for radiation qr increases. Figure 12 demonstrates the effect of scaled chemical reaction parameter  $\gamma$  on nanoparticle concentration. It is evident that nanoparticle volume fraction decreases with increase of chemical reaction parameters whereas the parameter shows no substantial changes on dimensionless velocity and temperature profiles. Also, from Table 1 it is evident that with increase in Lewis number Le, Prandlt number Pr and nonlinear stretching parameter n, the Nusselt and Sherwood numbers decrease. It shows from Table 2 that the increase in Magnetic parameters leads to skin friction coefficient increases. In view of Table 3, increase in chemical reaction parameter  $\gamma$  causes Nusselt number decreases whereas Sherwood numbers increases. A similar observation is witnessed for varying Radiation parameter R.

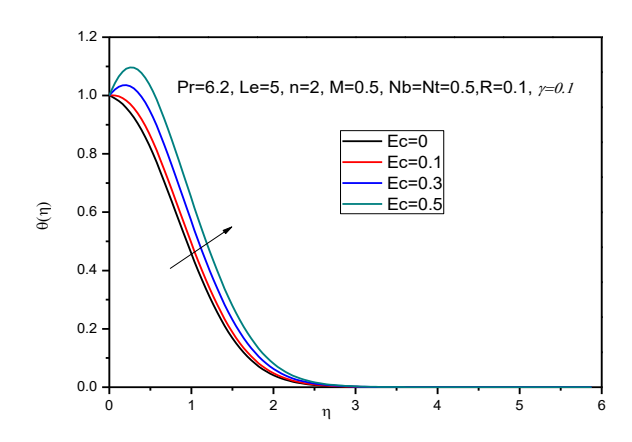


Figure 9. Effect of Ec on Dimensionless Temperature

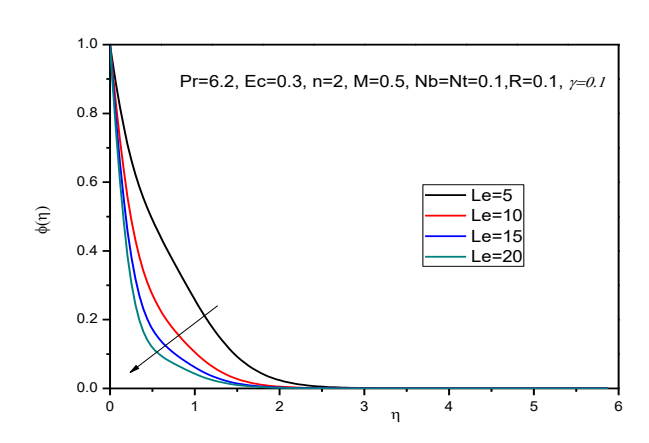


Figure 10. Effect of Le on Dimensionless Concentration

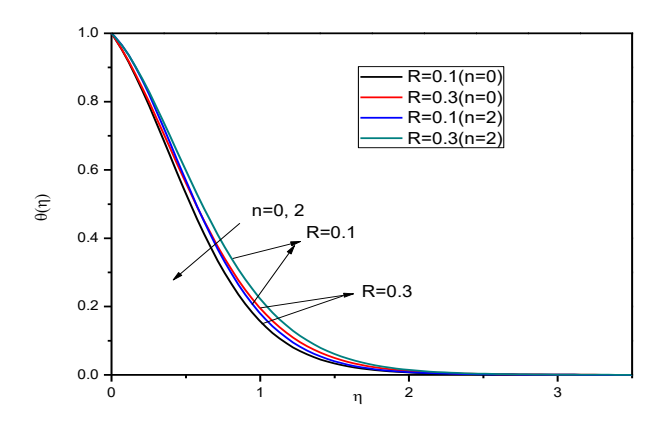


Figure 11. Effects of R and n on Dimensionless Temperature

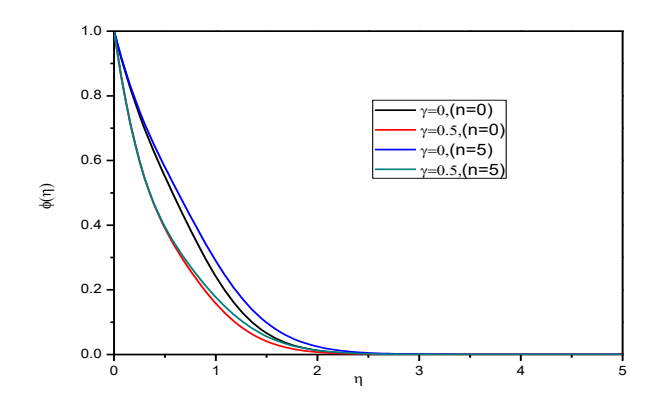


Figure 12. Effects of  $\gamma$  and n on Dimensionless Concentration

#### 4. CONCLUSIONS

The MHD boundary layer flow of nanofluids and heat transfer over a nonlinear stretching sheet; with chemical reaction and thermal radiation have been investigated semi-numerically. The various effects of parameters viz magnetic, the nonlinearity of stretching sheet, Brownian motion and thermophoresis parameters, viscous dissipation, chemical reaction, and radiation are debated in detail. The governing partial differential equations were transformed into non-linear ODEs through similarity transformations and these equations are solved semi-numerically via. HWCM. The following conclusions are drawn from the above study

- 1. As magnetic parameters increase, the dimensionless velocity temperature and concentration profiles increase. Also, the skin friction coefficient increases with an increase in magnetic parameters.
- 2. The dimensionless temperature and concentration profiles increase with the increase in the thermophoresis parameter.
- 3. As the Brownian motion parameter increases the dimensionless temperature profiles increase and concentration profiles decrease.
- 4. The temperature increases with viscous dissipation and concentration parameters decrease with an increase in Lewis number.
- 5. The temperature profiles increase with an increase in radiation and nonlinearly stretching parameters.
- 6. The concentration parameter decreases with an increase in a chemical reaction and nonlinearly stretching parameters.
- 7. The heat transfer rate decreases and the mass transfer rate increases with an increase in radiation and chemical reaction parameters.

# REFERENCE

- [1] B. C.Sakiadis, "Boundary layer behaviour on continuous solid surface, I: boundary layer equations for two-dimensional and axisymmetric flow", *Am. Inst. Chem. Eng. Journal*, vol. 7, pp. 26-28, 1961.
- [2] L. J. Crane, "Flow past a stretching plate", Z. Angew. Math. Phys., vol. 21, pp. 645-647,1972.
- [3] C. Y. Wang, "Free convection on a vertical stretching surface", ZAMM, vol. 69, pp 929-936, 1989.
- [4] K. Vajravelu, "Viscous flow over a nonlinear stretching sheet", *Appl. Math. Comput.* Vol. **124**, pp. 281-288, 2001.
- [5] T. Hayat, Z. Abbas and T. Javed, "Mixed convection flow of micropolar fluid over a non-linearly stretching sheet", *Physics Letters* A, vol. 372, pp. 637-647, 2008.
- [6] R. Cortell, "Flow of a viscous fluid over a nonlinearly (quadratic) porous stretching surface," in *Proc. Int. Conf. Future Inf. Technol. Manage. Sci. Eng.*, 2012, p. 14.
- [7] P. L. Sachdev, N. M. Bujurke and V.B. Awati, "Boundary value problems for third order nonlinear ordinary differential equations", *Studies in Applied Mathematics*, vol. 115, no. 3, pp. 303-318, 2005.

- [8] V.B. Awati, "Series solution of boundary layer flow of a nanofluid over a moving semi-infinite plate", *Journal of Nanofluids*, vol. 6, pp. 1-7, 2017.
- [9] S. U. S. Choi, "Enhancing thermal conductivity of fluids with nanoparticles," in *ASME Int. Mech. Eng. Congr.*, vol. 231, MD 66, pp. 99–105, 1995.
- [10] A. Malvandi, F. Hedayati and M. R. H. Nobari, "An analytical study on boundary layer flow and heat transfer of nanofluid induced by a non-linearly stretching sheet". *Journal of Applied Fluid Mechanics*, vol. 7, no.2, 375-384, 2014.
- [11] N. T. Eldable, E. M. A. Elbashbeshy and E. M. Elsaid, "Effects of Magnetic Field and Heat Generation on Viscous Flow and Heat Transfer over a Nonlinearly Stretching Surface in a Nanofluid", *International Journal of Applied Mathematics*, vol. 28, no.1, pp. 1130-1139, 2013.
- [12] O. D. Makinde and A. Aziz, "Boundary layer flow of a nanofluid past a stretching sheet with a convecyive boundary conditions", *International Journal of Thermal science*, vol. 50, pp. 1326-1332, 2011.
- [13] P. Rana and R. Bhargava, "Flow and heat transfer of a nanofluid over a nonlinearly stretching sheet: A numerical study," *Commun. Nonlinear Sci. Numer. Simul.*, vol. 17, no. 1, pp. 212–226, 2012.
- [14] F. Mabood, W. A. Khan and A.I.M. Ismail, "MHD boundary layer flow and heat transfer of nanofluids over a nonlinear stretching sheet: A numerical study", *Journal of Magnetism and magnetic materials*, vol. 374, pp. 569-576, 2015.
- [15] M. M. Rashidi et al., "Homotopy simulation of nanofluid dynamics from a nonlinearly stretching isothermal permeable sheet with transpiration," *Meccanica*, vol. 49, pp. 469–482, 2014.
- [16] W. A. Khan and I. Pop, "Boundary layer flow of a nanofluid past a stretching sheet". *International J. Heat and mass transfer*, vol. 53, pp. 2477-2483, 2010.
- [17] R. S. R. Gorla and I. Sidawi, "Free convection on a vertical stretching surface with suction and blowing". *Appl. Sci. Res.* Vol. 52, pp. 247-257, 1994.
- [18] D. Ramya, R. S. Raju and J. A. Rao, "Influence of chemical reaction on MHD Boundary layer flow of Nanofluid over a nonlinear stretching sheet with thermal radiation", *Journal of Nanofluids*, vol. 5, pp. 880-888, 2016.
- [19] V. B. Awati and N. Mahesh Kumar, "Analysis of forced convection boundary layer flow and heat transfer past a semi-infinite static and moving flat plate using nanofluids by Haar wavelets", *Journal of Nanofluids*, vol. 10, pp. 106-117, 2021.
- [20] V. B. Awati et al., "Haar wavelet scrutinization of heat and mass transfer features during the convective boundary layer flow of a nanofluid moving over a nonlinearly stretching sheet," *Partial Differ. Equ. Appl. Math.*, vol. 4, p. 100192, 2021.
- [21] P.S. Reddy and P. Sreedevi, "Impact of chemical reaction and double stratification on heat and mass transfer characteristics of nanofluid flow over porous stretching sheet with thermal radiation", *International. Journal of Ambient Energy*, vol. 43, pp. 1626–1636, 2022.
- [22] A. Rapits and C. Perdikis, "Viscous flow over a non-linearly stretching sheet in the presence of chemical reaction and magnetic fluid". *International Journal of nonlinear Mechanics*, vol. 41, pp. 527-529, 2006.
- [23] I. Anwar et al., "Chemical reaction and uniform heat generation or absorption effects on MHD stagnation-point flow of a nanofluid over a porous sheet," *World Appl. Sci. J.*, vol. 24, no. 10, pp. 1390–1398, 2013.
- [24] K. A. Helmy, "Solution of the boundary layer equation for a power law fluid in magneto-hydrodynamics", *ActaMech.* vol.102, pp. 25–37, 1994.
- [25] T. C. Chiam, "Hydromagnetic flow over a surface stretching with a power-law velocity", *International. J. Engineering Science*, vol. 33, pp. 429–435, 1995.

- [26] A. Ishak, R. Nazar and I. Pop, "Hydromagnetic flow and heat transfer adjacent to a stretching vertical sheet", *Heat and Mass Transfer*, vol. 44, pp.921–927, 2008.
- [27] S. S. Nourazar, M. H. Matin, and M. Simiari, "The HPM applied to MHD nanofluid flow over a horizontal stretching plate," *J. Appl. Math.*, pp. 1–17, 2011.
- [28] A. Zeeshan et al., "An investigation of porosity and magneto-hydrodynamic flow of non-Newtonian nanofluid in coaxial cylinders," *Int. J. Phys. Sci.*, vol. 7, no. 9, pp. 1353–1361, 2012.
- [29] A.J. Chamkha and A.M. Aly, "MHD free convection flow of a nanofluid past a vertical plate in the presence of heat generation or absorption effects", *Chemical Engineering Communications*, vol.198, pp. 425–441, 2011.
- [30] M. H. Matin, M.R.H. Nobari, and P. Jahangiri, "Entropy analysis in mixed convection MHD flow of nanofluid over a nonlinear stretching sheet", *J.Thermal Science and Technology*, vol. 7, no. 1, pp. 104–119, 2012.
- [31] V. B. Awati, Akash Goravar, N. Mahesh Kumar, and Chamkha, J. A., "Scrutinisation of Chebyshev collocation method for mass transfer on a continuous flat plate moving in parallel to a free stream in the presence of a chemical reaction", *International Journal of Ambient Energy*, DOI: 10.1080/01430750.2022.2127893, 2022.
- [32] A. Wakif, I. L. Animasaun, and R. Sehaqui, "A brief technical note on the onset of convection in a horizontal nanofluid layer of finite depth via Wakif-Galerkin weighted residuals technique (WGWRT)," in *Defect Diffus. Forum*, vol. 409, pp. 90–94, 2021.
- [33] U. Lepik, "Numerical solution of differential equations using Haar wavelets," *Math. Comput. Simul.*, vol. 68, no. 2, pp. 127–143, 2005.
- [34] U. Lepik and H. Hein, Haar wavelets: with applications, New York: Springer, 2014.
- [35] J. Majak, M. Pohlak, and M. Eerme, "Application of the Haar wavelet-based discretization technique to problems of orthotropic plates and shells," *Mech. Compos. Mater.*, vol. 45, no. 6, pp. 631–642, 2009.